3/5, to 2.5 to 3 × 10^{-10} cm^3 $molecule^{-1}$ s^{-1} at 20 K, which is within a factor of 2 of the measured rate coefficients for *cis*- and *trans*-butene.

The CASPT2 predictions for the saddle point energies, given in Table 1, correlate with the expectations, discussed earlier, based on the different values of (I.E. – E.A.). For ethene, the positive barrier leads to a low reactivity at low temperature. Propene and 1-butene are near ideal intermediate cases, with barriers within 1 kJ mol^{-1} of the reactants. For propene, the inner transition state strongly affects the rate coefficient even at 20 K, but the barrier is just low enough that, with tunneling, the rate coefficient does not decay to small values at low temperatures. For 1-butene, the rate coefficient rises with decreasing temperature but is still an order of magnitude below the long-range capture value at 20 K. For the other butenes, the ground-state barriers are strongly submerged (i.e., by 2 to 3 kJ mol^{-1}) and the addition rates increase rapidly with decreasing temperature, exceeding 10^{-10} cm^3 $molecule^{-1}$ s^{-1} by 20 K. The changing nature of the reaction with changing (I.E. – E.A.) is illustrated by the plots in Fig. 3 of the minimum energy path potentials as a function of the CO separation for the ground and first excited states in the $O(^3P)$ + ethene and $O(^3P)$ + *trans*-butene reactions.

The calculated rate coefficients for addition arising from the present two–transition state model are illustrated as dashed lines in Fig. 2. The calculations have been extended down to 1 K, and the results for the range from 10 to 1 K are given in fig. S1. For $O(^3P)$ + propene, the predicted rate coefficients are highly sensitive to the energy of the inner saddle point with a factor of 2 variation at 100 K for a 0.7 kJ mol^{-1} change. The CASPT2 predicted barrier was adjusted downward by 0.6 kJ mol^{-1} to obtain optimum agreement with experiment. For consistency, this adjustment was applied to the other reactions as well. For the butene cases, this adjustment has an insignificant effect on the predictions.

The remarkably good agreement between the theoretical predictions and experimental observations strongly validates the present two–transition state model. The calculations show that both the inner and outer transition states have an effect on the reaction kinetics throughout the 20 to 400 K range. At low temperatures the outer transition state dominates, whereas at high temperatures the inner transition state dominates. The increasing importance of the inner transition state with increasing temperature causes the negative temperature dependence between 200 and 20 K. The $O(^3P)$ + C_2H_4 reaction, where the positive barrier for the inner transition state dominates the kinetics at all temperatures, provides the only exception. The accurate treatment of both transition-state regions is a key prerequisite to understanding and predicting the kinetics of these reactions at low temperatures.

The agreement between experiment and theory found for the $O(^3P)$ + alkene reactions suggests two ways in which CASPT2 calculations of barrier heights might be used to estimate the possible importance in ISCs of other reactions between radicals and unsaturated molecules, depending on whether experimental information is available for the kinetics of the reaction in question—for example, a measured value of the rate coefficient at room temperature. If so, uncertainty in the ab initio calculations of the inner barrier height, which experience suggests might amount to a few kJ mol^{-1}, could be reduced by comparing theoretical and experimental values of the room-temperature rate coefficient so as to tune the potential energy at the inner transition state, and thereby improve the theoretical estimate of the low-temperature rate coefficients. As described above, we adopted this method with the use of the data for $O(^3P)$ + propene, although we found that the adjustment needed was quite small. In cases where no kinetic data exist, such as for the reactions of radicals with carbon chains (*19*), more reliance will have to be placed on the theory, guided by the success of the present calculations, or on the semi-empirical arguments concerning the value of (I.E. − E.A.). At the very least, these methods should provide guidance at the order-of-magnitude level, which is itself valuable at the present level of astrochemical modeling.

References and Notes

1. The acronym CRESU stands for Cinétique de Réaction en Ecoulement Supersonique Uniforme, or Reaction Kinetics in Uniform Supersonic Flow. The technique was originally developed by Rowe and his co-workers for the study of ion-molecule reactions (*20*).
2. I. W. M. Smith, *Angew. Chem. Int. Ed.* **45**, 2842 (2006).
3. I. W. M. Smith, A. M. Sage, N. M. Donahue, E. Herbst, D. Quan, *Faraday Discuss.* **133**, 137 (2006).
4. I. R. Sims *et al.*, *J. Chem. Phys.* **100**, 4229 (1994).
5. E. Herbst, *J. Phys. Chem. A* **109**, 4017 (2005).
6. I. W. M. Smith, E. Herbst, Q. Chang, *Mon. Not. R. Astron. Soc.* **350**, 323 (2004).
7. D. C. Clary, *Annu. Rev. Phys. Chem.* **41**, 61 (1990).
8. J. Troe, J. C. Lorquet, J. Manz, R. A. Marcus, M. Herman, *Adv. Chem. Phys.* **101**, 819 (1997).
9. Y. Georgievskii, S. J. Klippenstein, *J. Chem. Phys.* **122**, 194103 (2005).
10. E. E. Greenwald, S. W. North, Y. Georgievskii, S. J. Klippenstein, *J. Phys. Chem. A* **109**, 6031 (2005).
11. Y. Georgievskii, S. J. Klippenstein, *J. Phys. Chem. A* **111**, 3802 (2007).
12. J. S. Clarke, J. H. Kroll, N. M. Donahue, J. G. Anderson, *J. Phys. Chem. A* **102**, 9847 (1998).
13. R. J. Cvetanovic, *J. Phys. Chem. Ref. Data* **16**, 261 (1987).
14. R. B. Klemm, J. W. Sutherland, M. A. Wickramaaratchi, G. Yarwood, *J. Phys. Chem.* **94**, 3354 (1990).
15. T. L. Nguyen, L. Vereecken, X. J. Hou, M. T. Nguyen, J. Peeters, *J. Phys. Chem. A* **109**, 7489 (2005).
16. I. R. Sims *et al.*, *Chem. Phys. Lett.* **211**, 461 (1993).
17. Molpro, version 2006.1, a package of ab initio programs (www.molpro.net).
18. See supporting material on *Science* Online.
19. I. W. M. Smith, E. Herbst, J.-C. Loison, D. Quan, *Faraday Discuss.* **133**, 226 (2006).
20. B. R. Rowe, G. Dupeyrat, J. B. Marquette, P. Gaucherel, *J. Chem. Phys.* **80**, 4915 (1984).

21. Supported by the European Union via the award of a Marie Curie Chair (contract MEXC-CT-2004-006734, "Chemistry at Extremely Low Temperatures") (I.R.S.) and by grants from the Région de Bretagne, Rennes Métropole and the French Programme National de Physique Chimie du Milieu Interstellaire. The theoretical work (S.J.K. and Y.G.) was supported by the U.S. Department of Energy, Office of Basic Energy Sciences, Division of Chemical Sciences, Geosciences, and Biosciences. The portion at Argonne was supported under contract DE-AC02-06CH11357. Sandia is a multiprogram laboratory operated by Sandia Corp., a Lockheed Martin Company, for the U.S. Department of Energy under contract DE-AC04-94- AL8500.

Supporting Online Material

www.sciencemag.org/cgi/content/full/317/5834/102/DC1
Materials and Methods
SOM Text
Figs. S1 and S2
Tables S1 and S2
References

9 March 2007; accepted 9 May 2007
10.1126/science.1142373

Long-Lived Giant Number Fluctuations in a Swarming Granular Nematic

Vijay Narayan,[1]* Sriram Ramaswamy,[1,2] Narayanan Menon[3]

Coherently moving flocks of birds, beasts, or bacteria are examples of living matter with spontaneous orientational order. How do these systems differ from thermal equilibrium systems with such liquid crystalline order? Working with a fluidized monolayer of macroscopic rods in the nematic liquid crystalline phase, we find giant number fluctuations consistent with a standard deviation growing linearly with the mean, in contrast to any situation where the central limit theorem applies. These fluctuations are long-lived, decaying only as a logarithmic function of time. This shows that flocking, coherent motion, and large-scale inhomogeneity can appear in a system in which particles do not communicate except by contact.

Density is a property that one can measure with arbitrary accuracy for materials at thermal equilibrium simply by increasing the size of the volume observed. This is because a region of volume V, with N particles on average, ordinarily shows fluctuations with standard deviation ΔN proportional to $\sqrt{N}$, so that fluctuations in the number density go down as $1/\sqrt{V}$. Liquid crystalline phases of active or self-propelled particles (*1*–*4*) are different, with ΔN predicted (*2*–*5*) to grow faster than $\sqrt{N}$ and as fast as N in some cases (*5*), making density an ill-defined quantity even in the limit of a large system. These predictions show that flocking,

[1]Center for Condensed Matter Theory, Department of Physics, Indian Institute of Science, Bangalore 560012, India. [2]Condensed Matter Theory Unit, Jawaharlal Nehru Centre for Advanced Scientific Research, Bangalore 560064, India. [3]Department of Physics, University of Massachusetts, Amherst, MA 01003, USA.

*To whom correspondence should be addressed. E-mail: vj@physics.iisc.ernet.in

coherent motion, and giant density fluctuations are intimately related consequences of the orientational order that develops in a sufficiently dense grouping of self-driven objects with anisotropic body shape. This has substantial implications for biological pattern formation and movement ecology (*6*): The coupling of density fluctuations to alignment of individuals will affect populations as diverse as herds of cattle, swarms of locusts (*7*), schools of fish (*8*, *9*), motile cells (*10*), and filaments driven by motor proteins (*11*–*13*).

We report here that persistent giant number fluctuations and the coupling of particle currents to particle orientation arise in a far simpler driven system, namely, an agitated monolayer of rodlike particles shown in (*14*) to exhibit liquid crystalline order. These fluctuations have also been observed in computer simulations of a simple model of the flocking of apolar particles by Chaté *et al*. (*15*). The rods we used were cut to a length $l = 4.6 \pm 0.16$ (SEM) mm from copper wire of diameter $d = 0.8$ mm. The ends of the rods were etched to give them the shape of a rolling pin. The rods were confined in a quasi-two-dimensional cell 1 mm tall and with a circular cross-section 13 cm in diameter. The cell was mounted in the horizontal plane on a permanent magnet shaker and vibrated vertically at a frequency f = 200 Hz, with an amplitude, A, between 0.025 and 0.043 mm. The resultant dimensionless acceleration $\Gamma = (4\pi^2 f^2 A)/g$, where g is the acceleration due to gravity, varies between $\Gamma = 4$ and $\Gamma = 7$. We varied the total number of particles in the cell, N_{total}, between 1500 and 2820. N_{total} in each instance was counted by hand. The area fraction, ϕ, occupied by the particles is the total projected area of all the rods divided by the surface area of the cell. ϕ varies from 35% to 66%. Our experimental system is similar to those used to study the phase behavior of inelastic spheres (*16*, *17*). Galanis *et al*. (*18*) shook rods in a similar setup, albeit with much less confinement in the vertical direction. The particles were imaged with a digital camera (*19*).

The rods gain kinetic energy through frequent collisions with the floor and the ceiling of the cell. Because the axes of the particles are almost always inclined to the horizontal, these collisions impart or absorb momentum in the horizontal plane. Collisions between particles conserve momentum but also drive horizontal motion by converting vertical motion into motion in the plane. Interparticle collisions as well as particle-wall collisions are inelastic, and all particle motion would cease within a few collision times if the vibrations were switched off. The momentum of the system of rods is not conserved either, because the walls of the cell can absorb or impart momentum. The rods are apolar; that is, individual particles do not have a distinct head and tail that determine fore-aft orientation or direction of motion and can form a true nematic phase. The experimental system thus has all the physical ingredients of an active nematic (*1*–*4*).

The system is in a very dynamic steady state, with particle motion (movie S1) organized in macroscopic swirls. Swirling motions do not necessarily imply the existence of giant number fluctuations (*20*, *21*); however, particle motions in our system generate anomalously large fluctuations in density. Figure 1A shows a typical instantaneous configuration, and the Fig. 1B inset shows the orientational correlation function $G_2(r) = \langle \cos 2(\theta_i - \theta_j) \rangle$, where i,j run over pairs of particles separated by a distance r and oriented at angles θ_i and θ_j with respect to a reference axis. The angle brackets denote an average over all such pairs and about 150 images spaced 15 s apart in time. The data in the inset show that the systems with $N_{total} = 2500$ and $N_{total} = 2820$ display quasi–long-ranged nematic order, where $G_2(r)$ decays as a power of the separation, r. On the other hand, the system with $N_{total} = 1500$ shows only short-ranged nematic order, with $G_2(r)$ decaying exponentially with r. Details of the crossover between these two behaviors can be found in [Supporting Online Material (SOM) text]. Autocorrelations of the density field as well as of the orientation of a tagged particle decay to zero on much shorter time scales (SOM text), so we expect these images to be statistically independent. To quantify the number fluctuations, we extracted from each image the number of particles in subsystems of

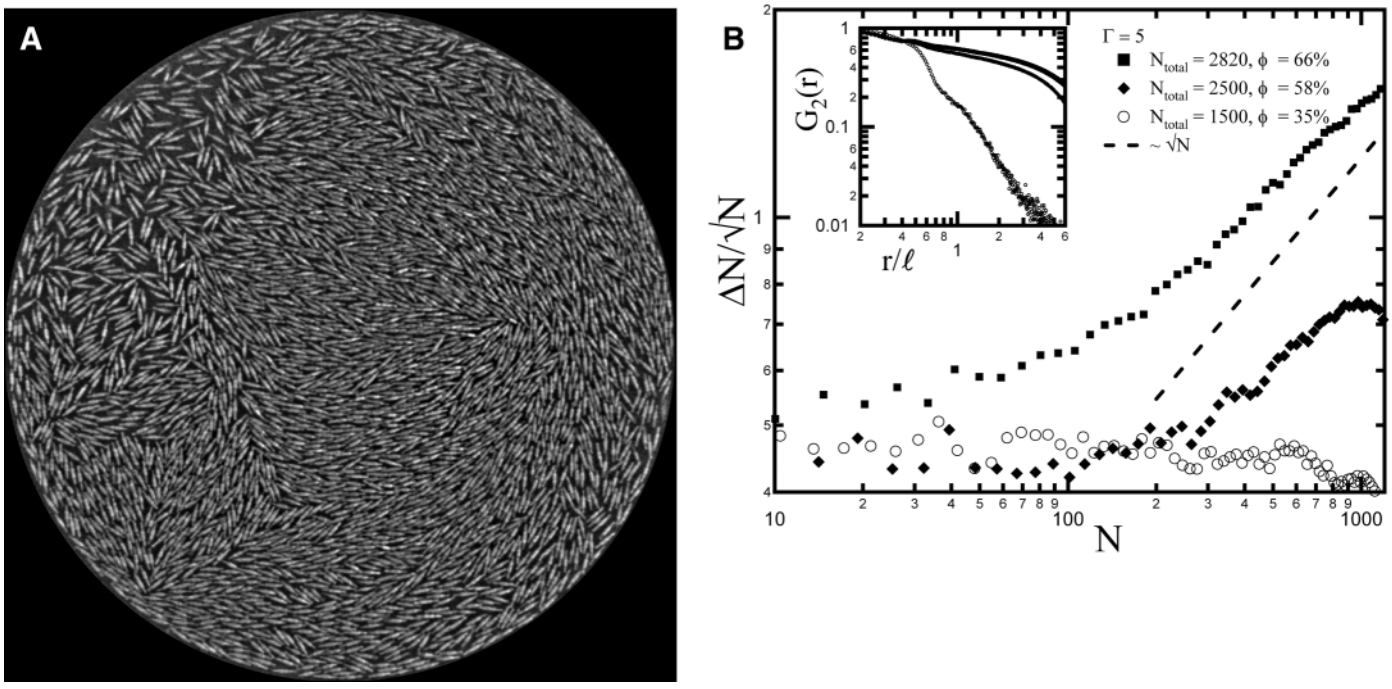

Fig. 1. Giant number fluctuations in active granular rods. (**A**) A snapshot of the nematic order assumed by the rods. There are 2820 particles (counted by hand) in the cell (area fraction is 66%) being sinusoidally vibrated perpendicular to the plane of the image, at a peak acceleration of $\Gamma = 5$. The sparse region at the top between 10 and 11 o'clock is an instance of a large density fluctuation. These take several minutes to relax and form elsewhere. (**B**) The magnitude of the number fluctuations (quantified by ΔN and normalized by $\sqrt{N}$) against the mean number of particles, for subsystems of various sizes. The number fluctuations in each subsystem are determined from images taken every 15 s over a period of 40 min (*19*). The squares represent the system shown in (A). It is a dense system where the nematic order is well developed. The magnitude of the scaled number fluctuations decreases in more dilute systems, where the nematic order is weaker (SOM text). Deviations from the central limit theorem result are still visible at an area fraction ≅ 58% (diamonds) but not at an area fraction ≅ 35% (circles). (Inset) The nematic-order correlation function as a function of spatial separation.

different size, defined by windows ranging in size from 0.1*l* by 0.1*l* to 12*l* by 12*l*. From a series of images we determined, for each subsystem size, the average *N* and the standard deviation, Δ*N*, of the number of particles in the window. For any system in which the number fluctuations obey the conditions of the central limit theorem (*22*), $\Delta N/\sqrt{N}$ should be a constant, independent of *N*. Figure 1B shows that, when the area fraction ϕ is large, $\Delta N/\sqrt{N}$ is not a constant. Indeed, for big enough subsystems, the data show giant fluctuations, Δ*N*, in the number of particles, growing far more rapidly than $\sqrt{N}$ and consistent with a proportionality to *N*. For smaller average number density, where nematic order is poorly developed, this effect disappears, and $\Delta N/\sqrt{N}$ is independent of *N*, as in thermal equilibrium systems. The roll-off in $\Delta N/\sqrt{N}$ at the highest values of *N* is a finite-size effect: For subsystems that approach the size of the entire system, large number fluctuations are no longer possible because the total number of particles in the cell is held fixed.

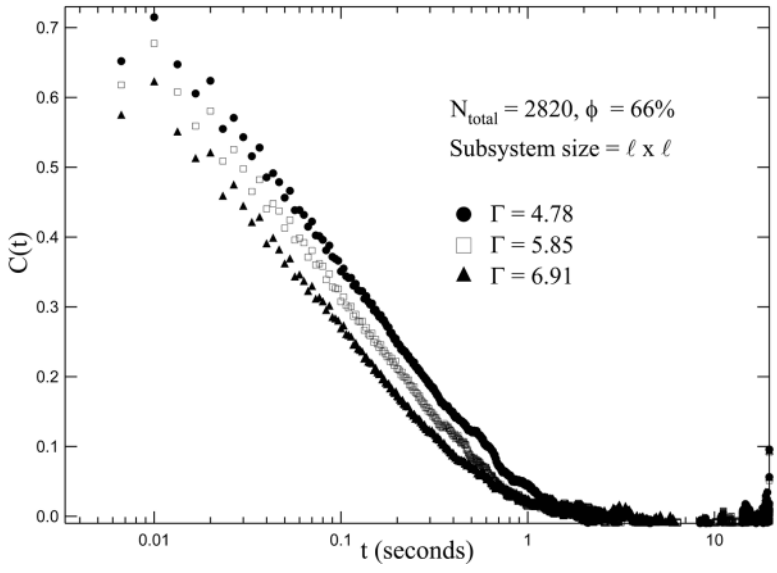

Fig. 2. The logarithmic dependence of the local density autocorrelation, $C(t) = \langle\varphi(0)\varphi(t)\rangle$ [$\varphi(t)$ is the deviation from the mean of the instantaneous number density of particles], is a direct consequence (SOM text), and hence a clear signature, of the large density fluctuations in the system. It is remarkable that such a local property reflects the dynamics of the entire system so strongly. It is seen that increasing Γ shortens the decay time. This is consistent with the fact that the magnitude of the giant number fluctuations grows with the nematic order (SOM text).

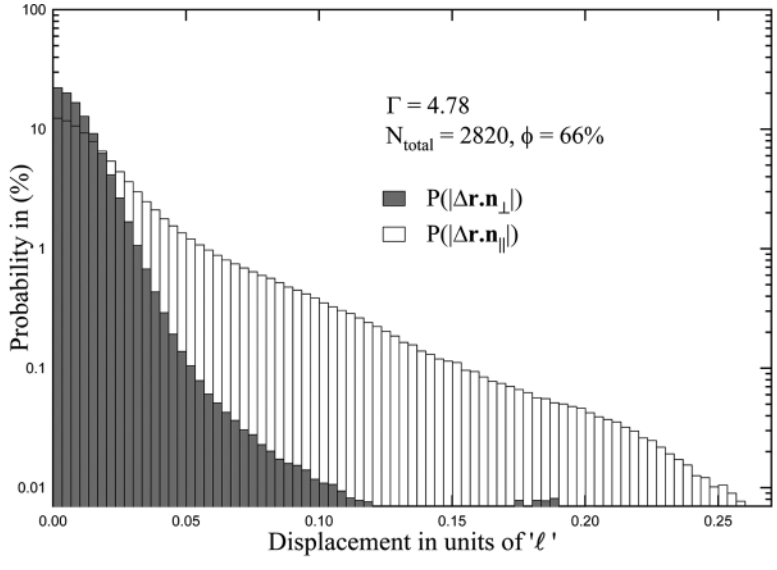

Fig. 3. The microscopic origin of the macroscopic density fluctuations. The probability distribution of the magnitude of the displacement along and transverse to the particle's long axis over an interval of 1/300 of a second shows that short time motion of the rods is anisotropic even at the time scale of the collision time. This anisotropy is explicitly forbidden in equilibrium systems by the equipartition theorem.

We examined a subsystem of size *l* by *l* (i.e., one rod length on a side) and obtained a time series of particle number, *N*(*t*), by taking images at a frame rate of 300 frames per s. From this we determined the temporal autocorrelation, *C*(*t*), of the density fluctuations. *C*(*t*) decays logarithmically in time (Fig. 2), unlike the much more rapid t^{-1} decay of random, diffusively relaxing density fluctuations in two dimensions. Thus, the density fluctuations are not only anomalously large in magnitude but also extremely long-lived. Indeed, these two effects are intimately related: An intermediate step in the theoretical argument (*5*) that predicts giant number fluctuations shows that density fluctuations at a wave number *q* have a variance proportional to q^{-2} and decay diffusively. This leads to the conclusion (SOM text) that in the time regime intermediate between the times taken for a density mode to diffuse a particle length and the size of the system, the autocorrelation function of the local density decays only logarithmically in time. Although the observations agree with the predicted logarithmic decay, we cannot as yet make quantitative statements about the coefficient of the logarithm. We note that the size of subsystem is below the scale of subsystem size at which the standard deviation has become proportional to the mean. In flocks and herds as well, measuring the dynamics of local density fluctuations will yield crucial information regarding the entire system's dynamics and can be used to test the predictions of Toner and Tu (*2*, *3*).

What are the microscopic origins of the giant density fluctuations? Both in active and in equilibrium systems, particle motions lead to spatial variations in the nematic ordering direction. However, in active systems alone, such bend and splay of the orientation are predicted (*5*) to select a direction for coherent particle currents. These curvature-driven currents in turn engender giant number fluctuations. We find qualitative evidence for curvature-induced currents in the flow of particles near topological defects (SOM text). In the apolar flocking model of (*15*), particles move by hopping along their axes and then reorienting, with a preference to align parallel to the average orientation of particles in their neighborhood. Requiring that the hop be along the particle axis was sufficient to produce giant number fluctuations in the nematic phase of the system. It was further suggested in (*15*) that the curvature-induced currents of (*5*), although not explicitly put into their simulation, must emerge as a macroscopic consequence of the rules imposed on microscopic motion. This suggestion is substantiated by the work of Ahmadi *et al.* (*23*), who started from a microscopic model of molecular motors moving preferentially along biofilaments and showed by coarse-graining this model that the equation of motion for the density of filaments contains precisely the term in (*5*) responsible for curvature-induced currents.

In our experiments, we found anisotropy at the most microscopic level of single particle mo-

tion, even at time scales shorter than the vibration frequency, f. In equilibrium, the mean kinetic energies associated with the two in-plane translation degrees of freedom of the particle are equal, by the equipartition theorem, even if the particle shape is anisotropic. Figure 3 is a histogram of the magnitude of particle displacements over a time corresponding to the camera frame rate [1/300 s, or $(2/3)f^{-1}$]. The displacement along and perpendicular to the axis of the rod are displayed separately, showing that a particle is about 2.3 times as likely to move along its length as it is to move transverse to its length. Because the period of the imposed vibration (f^{-1}) sets the scale for the mean free time of the particles, this shows that the motion of the rods is anisotropic even at time scales less than or comparable to the mean free time between collisions.

We have thus presented an experimental demonstration of giant, long-lived number fluctuations in a two-dimensional active nematic. The particles in our driven system do not communicate except by contact, have no sensing mechanisms, and are not influenced by the spatially varying pressures and incentives of a biological environment. This reinforces the view that, in living matter as well, simple, nonspecific interactions can give rise to large spatial inhomogeneity. Equally important, these effects offer a counterexample to the deeply held notion that density is a sharply defined quantity for a large system.

References and Notes

1. T. Vicsek, A. Czirok, E. Ben-Jacob, I. Cohen, O. Shochet, *Phys. Rev. Lett.* **75**, 1226 (1995).
2. J. Toner, Y. Tu, *Phys. Rev. Lett.* **75**, 4326 (1995).
3. J. Toner, Y. Tu, *Phys. Rev. E* **58**, 4828 (1998).
4. J. Toner, Y. Tu, S. Ramaswamy, *Ann. Phys.* **318**, 170 (2005).
5. S. Ramaswamy, R. A. Simha, J. Toner, *Europhys. Lett.* **62**, 196 (2003).
6. C. Holden, *Science* **313**, 779 (2006).
7. J. Buhl *et al.*, *Science* **312**, 1402 (2006).
8. N. C. Makris *et al.*, *Science* **311**, 660 (2006).
9. C. Becco *et al.*, *Physica A (Amsterdam)* **367**, 487 (2006).
10. B. Szabó *et al.*, *Phys. Rev. E* **74**, 061908 (2006).
11. F. Nédélec, T. Surrey, A. C. Maggs, S. Leibler, *Nature* **389**, 305 (1997).
12. D. Bray, *Cell Movements: From Molecules to Motility* (Garland, New York, 2001).
13. H. Gruler, U. Dewald, M. Eberhardt, *Eur. Phys. J. B* **11**, 187 (1999).
14. V. Narayan, N. Menon, S. Ramaswamy, *J. Stat. Mech.* **2006**, P01005 (2006).
15. H. Chaté, F. Ginelli, R. Montagne, *Phys. Rev. Lett.* **96**, 180602 (2006).
16. A. Prevost, D. A. Egolf, J. S. Urbach, *Phys. Rev. Lett.* **89**, 084301 (2002).
17. P. M. Reis, R. A. Ingale, M. D. Shattuck, *Phys. Rev. Lett.* **96**, 258001 (2006).
18. J. Galanis, D. Harries, D. L. Sackett, W. Losert, R. Nossal, *Phys. Rev. Lett.* **96**, 028002 (2006).
19. Materials and methods are available on *Science* Online.
20. D. L. Blair, T. Neicu, A. Kudrolli, *Phys. Rev. E* **67**, 031303 (2003).
21. I. Aranson, D. Volfson, L. S. Tsimring, *Phys. Rev. E* **75**, 051301 (2007).
22. W. Feller, *An Introduction to Probability Theory and its Applications* (Wiley, New York, ed. 3, 2000), vol. I.
23. A. Ahmadi, T. B. Liverpool, M. C. Marchetti, *Phys. Rev. E* **74**, 061913 (2006).

24. We thank V. Kumaran, P. Nott, and A. K. Raychaudhuri for generously letting us use their experimental facilities. V.N. thanks S. Kar for help with some of the experiments. V.N. and S.R., respectively, thank the Council for Scientific and Industrial Research, India, and the Indo-French Centre for the Promotion of Advanced Research (grant 3504-2) for support. The Centre for Condensed Matter Theory is supported by the Department of Science and Technology, India. N.M. acknowledges financial support from NSF under grants DMR 0606216 and 0305396.

Supporting Online Material

www.sciencemag.org/cgi/content/full/317/5834/105/DC1
Materials and Methods
SOM Text
Figs. S1 to S6
Movies S1 and S2

25 January 2007; accepted 31 May 2007
10.1126/science.1140414

Trench-Parallel Anisotropy Produced by Foundering of Arc Lower Crust

Mark D. Behn,[1]* Greg Hirth,[1] Peter B. Kelemen[2]

Many volcanic arcs display fast seismic shear-wave velocities parallel to the strike of the trench. This pattern of anisotropy is inconsistent with simple models of corner flow in the mantle wedge. Although several models, including slab rollback, oblique subduction, and deformation of water-rich olivine, have been proposed to explain trench-parallel anisotropy, none of these mechanisms are consistent with all observations. Instead, small-scale convection driven by the foundering of dense arc lower crust provides an explanation for the trench-parallel anisotropy, even in settings with orthogonal convergence and no slab rollback.

The origin of seismic anisotropy in Earth's upper mantle is attributed to the deformation-induced alignment of olivine crystals. Anisotropy can be quantified through measurements of shear-wave splitting, in which the orientation and strength of the anisotropy are estimated by measuring the polarization direction of the fastest-propagating shear wave and the delay time between the arrivals of the fastest and slowest shear waves. The relation between anisotropy and mantle flow is seen clearly at mid-ocean ridges, where fast polarization directions are oriented parallel to the spreading direction (*1*). This observation is consistent with a model in which the olivine *a* axis aligns with the transport direction inferred for corner flow beneath a ridge (*2*, *3*).

Beneath volcanic arcs, shear-wave splitting measurements frequently show fast polarization directions parallel to the strike of the arc (*4*–*6*), which rotate to a trench-normal orientation in the back-arc (*5*, *6*). Direct comparison of delay times from teleseismic *SKS* phases (which propagate through the entire mantle) (*7*) and local *S* phases generated in the subducting slab (*8*) indicates that a substantial fraction of the trench-parallel anisotropy resides in the mantle wedge above the slab (Fig. 1). Splitting measurements from local events also show strong along-arc variability in the orientation of anisotropy, with certain regions being characterized by trench-parallel anisotropy and other regions displaying more variable fast polarization directions (Fig. 1) (*8*–*10*). In contrast, two-dimensional (2D) models of slab-driven corner flow, like those invoked to explain the pattern of anisotropy at mid-ocean ridges, predict trench-normal anisotropy in the mantle wedge at subduction zones (*11*).

Deformation experiments on olivine aggregates show that the lattice preferred orientation (LPO) changes as a function of water content, stress, and temperature (*12*, *13*). Particularly intriguing is the observation of LPO controlled by the dominance of slip on the (010)[001] slip system (i.e., the B-type system). In this regime, which is predicted to dominate at high water content and low temperature/high stress, fast polarization directions are perpendicular to the flow direction (they are trench-parallel for 2D slab-driven corner flow). However, although numerical models (*14*) predict B-type fabric in the fore-arc, it is not predicted beneath the arc or in the back-arc, where trench-parallel anisotropy is often observed.

An alternative explanation for trench-parallel anisotropy is 3D flow in the mantle wedge due to oblique convergence or slab rollback (*11*, *15*). Yet, these models do not explain trench-parallel anisotropy observed in settings with nearly orthogonal convergence and little rollback (Fig. 1) (*4*, *8*). Another potential source of 3D flow in the mantle wedge is buoyancy-driven flow resulting from the foundering of high-density mafic and ultramafic cumulates into the underlying mantle (*16*). At conditions appropriate for arc lower crust (800° to 1000°C and 1 GPa) (*17*), many crustal

[1]Department of Geology and Geophysics, Woods Hole Oceanographic Institution, Woods Hole, MA 02543, USA. [2]Lamont Doherty Earth Observatory, Columbia University, Palisades, NY 10964, USA.

*To whom correspondence should be addressed. E-mail: mbehn@whoi.edu

Long-Lived Giant Number Fluctuations in a Swarming Granular Nematic

Vijay Narayan, Sriram Ramaswamy and Narayanan Menon

Science **317** (5834), 105-108.
DOI: 10.1126/science.1140414